Monthly Notices
of the
ROYAL ASTRONOMICAL SOCIETY

MNRAS **480,** 2508–2520 (2018)
Advance Access publication 2018 July 27

doi:10.1093/mnras/sty2021

GASP – X. APEX observations of molecular gas in the discs and in the tails of ram-pressure stripped galaxies

A. Moretti,[1⋆] R. Paladino,[2⋆] B. M. Poggianti,[1⋆] M. D'Onofrio,[3] D. Bettoni,[1] M. Gullieuszik,[1] Y. L. Jaffé,[4] B. Vulcani,[1,5] G. Fasano,[1] J. Fritz[6] and K. Torstensson[7]

[1]*INAF – Astronomical Observatory of Padova, Vicolo dell'Osservatorio 5, I-35122 Padova, Italy*
[2]*INAF – Istituto di Radioastronomia and Italian ALMA Regional Centre, via P. Gobetti 101, I-40129 Bologna, Italy*
[3]*Department of Physics and Astronomy, University of Padova, Vicolo dell'Osservatorio 5, I-35122 Padova, Italy*
[4]*Instituto de Física y Astronomía, Universidad de Valparaíso, Avda. Gran Bretaña 1111, Valparaíso, Chile*
[5]*School of Physics, The University of Melbourne, Swanston St and Tin Alley Parkville, VIC 3010, Australia*
[6]*Instituto de Radioastronomía y Astrofísica, UNAM, Campus Morelia, A.P. 3-72, C.P. 58089, Mexico*
[7]*European Southern Observatory, Karl-Schwarzschild-Str. 2, D-85748 Garching bei Munchen, Germany*

Accepted 2018 July 20. Received 2018 July 18; in original form 2018 March 15

ABSTRACT

Jellyfish galaxies in clusters are key tools to understand environmental processes at work in dense environments. The advent of integral field spectroscopy has recently allowed to study a significant sample of stripped galaxies in the cluster environment at $z \sim 0.05$, through the GAs Stripping Phenomena in galaxies with MUSE (GASP) survey. However, optical spectroscopy can only trace the ionized gas component through the Hα emission that can be spatially resolved on kpc scale at this redshift. The complex interplay between the various gas phases (ionized, neutral, and molecular) is, however, yet to be understood. We report here the detection of large amounts of molecular gas in the discs of four jellyfish galaxies from the GASP sample with stellar masses $\sim 3.5 \times 10^{10}$–3×10^{11} M$_\odot$, showing strong stripping. Moreover, a significant detection is found in two of the stripped tails, and in regions neighbouring the galaxy discs in all four galaxies, while the detection of the furthest regions in two of our galaxies is only tentative. The mass of molecular gas that we measure in the tails amounts to several 10^9 M$_\odot$, and the total mass of molecular gas ranges between 15 and 100 per cent of the galaxy stellar mass. We find a clear correlation between the ionized gas emission Hα and the amount of molecular gas. The CO velocities measured from APEX data are not always coincident with the underlying Hα emitting knots, and the derived star formation efficiencies appear to be very low.

Key words: galaxies: clusters: general – galaxies: evolution – galaxies: formation – galaxies: star formation.

1 INTRODUCTION

Galaxy evolution is strictly linked both to the environment in which galaxies reside and to their mass (Dressler 1980; Cowie et al. 1996; Peng et al. 2010). In particular, galaxies in clusters are more efficiently quenched than their analogous in the field (Tanaka et al. 2004; Cucciati et al. 2006; Poggianti et al. 2006; Guglielmo et al. 2015). Among the various mechanisms at play in dense environments (Boselli & Gavazzi 2006), some are influencing both the gas and the stellar populations in galaxies and are due to gravitational/tidal interactions (Spitzer & Baade 1951; Toomre & Toomre 1972; Merritt & D. 1983; Byrd & Valtonen 1990; Moore et al. 1999), while others involve only the gaseous components, resulting from the hydrodynamical interaction between the hot intra-cluster medium (ICM) and the gas in the disc/halo of galaxies (Larson, Tinsley & Caldwell 1980; Balogh, Navarro & Morris 2000). Among the latter, ram-pressure stripping (RPS, Gunn & Gott 1972) seems to be favoured in shaping galaxy properties in clusters (Chung et al. 2009; Gavazzi et al. 2013; Jaffe et al. 2015; Yoon et al. 2017).

In order to build a statistically significant sample of cluster galaxies with evidence of RPS (either in action, or already in an advanced stage, leaving as signatures truncated Hα discs), we started a survey of candidate jellyfish galaxies (i.e. galaxies showing optical signatures of unilateral debris/disturbed morphology, suggestive of gas-only removal processes) in low-redshift clusters (Poggianti et al.

⋆ E-mail: alessia.moretti@oapd.inaf.it (AM); rosita.paladino@inaf.it (RP); bianca.poggianti@inaf.it (BMP)

2016). From this sample, we identified as targets galaxies with clear optical asymmetric morphologies suggestive of ram–pressure stripping and observed them with the MUSE spectrograph at VLT (GASP,[1] GAs Stripping Phenomena in galaxies with MUSE, Poggianti et al. 2017b), including also in the observed sample field and groups galaxies with similar characteristics. Our first results reveal that large amount of gas can be stripped from the galaxy main body due to the interaction with the ICM. Hα knots have been found in all the GASP cluster galaxies (Bellhouse et al. 2017; Fritz et al. 2017; Gullieuszik et al. 2017; Poggianti et al. 2017b; Moretti et al. 2018), as well as in NGC 4388 (Yagi et al. 2013) and other Virgo cluster regions (Gerhard et al. 2002; Cortese et al. 2004) and in other jellyfish galaxies (Fumagalli et al. 2014; Fossati et al. 2016; Consolandi et al. 2017), and have been associated with star formation (SF) in the galaxy tails. However, since SF is known to take place in regions where cold gas is present, complementary observations measuring the amount and location of molecular hydrogen are needed in order to assess if there is extraplanar molecular gas and whether this gas has been formed *in situ* or if it has been stripped from the galaxy body (Jáchym et al. 2014; Kenney & Young 1989; Boselli et al. 1997). In normal galaxies, the molecular gas tends to be concentrated in the central regions, displaying a surface density decreasing with radius (Young & Scoville 1991; Wong & Blitz 2002), while H I discs seem to be much more extended than the optical ones (Bosma 1981). RPS would then strip mainly neutral atomic gas from the discs, producing the H I morphologies detected in Virgo and Coma (Kenney, van Gorkom & Vollmer 2004; Chung et al. 2009; Kenney et al. 2013; Serra et al. 2013). This gas then appears as ionized and revealed through the Hα emission (Gavazzi et al. 2001; Sun, Donahue & Voit 2007; Yagi et al. 2007, 2010; Fossati et al. 2012; Yagi et al. 2017), and finally gets heated to the cluster X-rays temperature (Sun et al. 2010).

The cold molecular gas phase has been detected so far in only four stripped galaxies mainly through CO emission (Dasyra et al. 2012; Jáchym et al. 2014; Verdugo et al. 2015; Jachym et al. 2017). Further evidence is found in the Virgo cluster, where molecular gas in the tails of a dwarf galaxy (upper limits only, Jáchym et al. 2013) and in the vicinity of the disc of two galaxies (Vollmer et al. 2008) has been detected. High-resolution CO data in three Virgo galaxies (Lee et al. 2017) have shown that the overall distribution of cold gas seems to follow the stripped H I, but no clear sign of molecular gas stripping has been detected.

The presence of CO emission in galaxy outskirts is somewhat surprising, given its overall distribution in galaxy discs, and remains unclear whether this cold gas component could have been stripped together with the neutral one, or if, instead, it has been formed locally after the gas was stripped. In fact, the survival of dense gas clouds in the ICM is difficult to understand, unless processes like heat conduction, turbulence, and the ionizing X-rays radiation show low efficiencies. Finally, in order to understand how RPS proceeds, we must understand the efficiency of SF in the tails. This is usually derived from the comparison between the surface densities of the star formation rate (SFR) and the molecular gas content, which shows a roughly linear relation, the so called Schmidt–Kennicutt relation (Schmidt 1959; Kennicutt 1998). This relation, however, is not universal, as in extreme conditions (such as galaxy centres, galaxy outskirts, and low-surface-brightness galaxies) it can fail (Boissier et al. 2008; Dessauges-Zavadsky et al. 2014; Casasola et al. 2015).

[1] http://web.oapd.inaf.it/gasp

Normal disc galaxies at low redshift show average depletion times (the time-scale to convert all the molecular gas reservoir in a given region into stars at the current SFR), of $\tau_{\rm dep} \sim 1$–2 Gyr (Bigiel et al. 2008, 2011), while galaxies extending towards the green valley/passive region of the SFR versus stellar mass ($M_\star$) plane (Saintonge et al. 2017) have depletion times up to $\sim$10 Gyr. Finally, low SF efficiencies have been found both in the extended UV disc of M63 (Bigiel et al. 2010; Dessauges-Zavadsky et al. 2014) and in low-surface-brightness galaxies (Boissier et al. 2008).

As for ram-pressure stripped galaxies, the detection of molecular gas along the tails is relatively recent, and indicates a low SF efficiency. The first detection of an abundant molecular gas component in a tail was reported by Jáchym et al. (2014) in the galaxy ESO 137 − 001 in the Norma cluster, with a stellar mass ($\sim 10^9$ M$_\odot$) that is comparable with the ionized gas mass. The two gas phases together almost completely account for the missing gas mass in the galaxy disc. In the Virgo cluster, lower quantities of molecular gas have been found in the long tail ($\sim$70 kpc) of NGC 4388 (Verdugo et al. 2015), and only upper limits of CO emission have been reported for IC 3418 (Jáchym et al. 2013). More recently, Jachym et al. (2017) found large amounts ($\sim 10^9$ M$_\odot$) of molecular gas in the very long and collimated tail ($\sim$50 kpc) of the galaxy D100 in the Coma cluster with the IRAM 30-m telescope. Somewhat surprisingly, the mass of ionized gas is 5–10 times smaller, making the cold gas the dominant component of the tail. Moreover, the CO velocities display a gradient along the tail, and a differential displacement with respect to the ionized gas velocities, suggesting that the densest gas clumps might be less accelerated by the ram pressure than the ionized gas.

The derived depletion times in these tails are longer than the Hubble time, meaning that most of the molecular gas will ultimately join the ICM without forming stars. As for the origin of the CO, it is speculated that at such large distances from the galaxy the CO cannot have been stripped, and its origin must be due to *in situ* formation from the H I stripped gas. This means that probably the hot ICM is not able to prevent gas cooling and condensation along the tail. In particular, Jachym et al. (2017) argued that while RPS might be able to directly strip gas as dense as $\sim$50 M$_\odot$ pc^{-2} down to 1 kpc disc radius, it might fall short in stripping denser gas present in the form of giant molecular clouds (GMCs). If this is true, then the GMCs would be gradually removed by the effects of RPS. Simulations (Tonnesen & Bryan 2009, 2012) predict, in fact, that the densest clouds cannot be entirely removed by the RPS, and are therefore disrupted. The new stars born in the tails are probably created from less dense gas that has been able to cool and subsequently condense in the tail. Overall, the complex interplay between the density/temperature conditions of the stripped gas and the ICM determines both how long is the process of mixing into the ICM and the distribution of new stars in the tails.

In order to get a clearer picture of the multiple gas phases in ram-pressure stripped galaxies, we obtained APEX (the Atacama Pathfinder Experiment) ^{12}CO(2 − 1) data for four galaxies of the GASP sample, JO201, JO204, JO206, and JW100 located in the clusters A85, A957, IIZW108, and A2626, respectively. Galaxy stellar masses range from $\sim 3.55 \times 10^{10}$ M$_\odot$ to $\sim 3.0 \times 10^{11}$ M$_\odot$, as derived from integrated galaxy spectra extracted from the MUSE cube and using the Chabrier (2003) initial mass function (IMF), while cluster masses (Moretti et al. 2017) range between 0.38 and 1.58 $\times 10^{15}$ M$_\odot$ (see Table 1). We refer the reader to the dedicated GASP papers (Bellhouse et al. 2017; Gullieuszik et al. 2017; Poggianti et al. 2017b) for more details on the sampled galaxies.

Table 1. Target galaxies.

Galaxy	Cluster	Stellar mass (10^{10} $M_\odot$)	Redshift	Cluster mass (10^{15} $M_\odot$)
JO201[a]	A85	3.55	0.045	1.58
JO204[b]	A957	4	0.042	0.44
JO206[c]	IIZW108	9	0.051	0.38
JW100	A2626	30	0.061	0.40

[a]Bellhouse et al. (2017); [b]Gullieuszik et al.(2017); [c]Poggianti et al. (2017b)

Table 2. Observations log.

Gx	Pos.	RA	Dec.	T_{ON} (min)	Frequency (MHz)
JO201	A	00:41:30.32	−09:15:45.8	30	220 680.2
JO201	B	00:41:31.07	−09:15:23.5	175	220 680.2
JO201	C	00:41:32.80	−09:15:20.2	30	220 680.2
JO201	D	00:41:32.00	−09:15:43.8	62	220 680.2
JO201	E	00:41:33.00	−09:16:03.6	32	220 680.2
JO201	F	00:41:31.31	−09:16:05.4	66	220 680.2
JO204	A	10:13:46.34	−00:54:53.5	26	221 152.2
JO204	B	10:13:46.17	−00:54:39.4	68	221 152.2
JO204	C	10:13:48.10	−00:54:56.5	145	221 152.2
JO206	A	21:13:47.6	02:28:28.2	9	219 288.5
JO206	B	21:13:45.7	02:28:44.2	27	219 288.5
JO206	C	21:13:43.8	02:28:26.2	93	219 288.5
JO206	D	21:13:42.80	02:28:49.2	139	219 288.5
JW100	A	23:36:24.55	21:09:05.7	12	217 258.7
JW100	B	23:36:23.73	21:08:44.6	71	217 258.7

2 APEX OBSERVATIONS

The observations of the four selected galaxies of the GASP sample have been taken with the 12-m antenna APEX, as part of two programs E-098.B-0657A-2016 in December 2016, and E-099.B-0063A-2017, from 2017 April to July.

We observed the ^{12}CO(2 − 1) transition (ν_{rest} = 230.538 GHz), using the Swedish heterodyne facility instrument (Vassilev et al. 2008), and the eXtended Fast Fourier Transform Spectrometer (XFFTS) back-end, tuned to the CO line redshifted frequencies for each target.

At the observed frequencies (220 GHz), the FWHM of the APEX primary beam is 28 arcsec, corresponding to scales from ∼25 to ∼30 Kpc for the different targets. Multiple pointings have been observed for each target, in order to cover the main body, as well as different regions in the tails, at different distances from the galaxy. Their locations are listed in Table 2, and shown in Figs 1–4. The observations have been performed in a symmetric Wobbler switching mode, with maximum separation between the ON and OFF-beam of 150 arcsec.

Observations have been taken in different sessions with different weather conditions, with precipitable water vapour ranging from 0.7 to 3 mm.

2.1 Data reduction

The spectra calibrated by the APEX on-line calibration pipeline (in antenna temperature scale; T_A^*) have been further reduced using the standard procedure with the program CLASS from the GILDAS software package.[2] Bad scans were flagged and the spectra have been aligned in the same velocity frame, and smoothed to a common spectral resolution of 80 km s^{-1}. Some of the pointings show emissions strong enough to be detected with S/N > 3 also at higher spectral resolution. First-order baselines, defined in a line-free band about 2000 km s^{-1} wide, have been subtracted to the spectra. The antenna temperatures have been converted to main-beam brightness temperatures ($T_{mb} = T_A^*/\eta_{mb}$), using $\eta_{mb} = 0.75$.

The typical levels of rms noise obtained in channels 80 km s^{-1} wide range from 0.5 to 1.2 mK.

The list of the observed positions with the on-source observing times and the observed frequency is provided in Table 2. The observed frequency corresponds to the galaxy central redshift, as derived from the MUSE data cubes.

The peak temperature (main-beam brightness temperature, T_{mb}^*) as well as the width and the position of the CO line have been derived initially with a single Gaussian fit, and with a multiple gaussian component where needed. CO fluxes have been calculated assuming a conversion factor of $S_\nu/T_{mb} = 39$ Jy beam^{-1} K^{-1} for the APEX telescope. The signal-to-noise ratio (S/N) of our measurements has been derived as the peak temperature of the fit over the rms of the baseline. The results of the fitting procedure are given in Table 3.

3 MUSE DATA

Within the GASP project (Poggianti et al. 2017b), we observed so far ∼100 galaxies showing more or less pronounced signatures of gas stripping phenomena in action. For each galaxy, we have been able to derive gas and stellar properties from the single spaxels (smoothed on a 0.7–1.3 kpc scale, depending on the galaxy redshift), as well as from the galaxy integrated spectra. In the following Figs 1–4, we show in the two upper panels the white light image obtained by integrating the MUSE data cubes over the entire wavelength range of each target galaxy (top left-hand panels) and the stellar kinematics (top right-hand panels) derived from the MUSE data cubes. The stellar kinematics have been measured in Voronoi binned regions with a S/N of 10 (Cappellari & Copin 2003) using the PPXF software (Cappellari & Emsellem 2003), as described in Poggianti et al. (2017b). Moreover, we used the Hα images extracted from the MUSE data cubes to locate the star-forming knots both in the galaxy disc and along the tails. The knots positions have been identified as local minima on the Hα image filtered using a laplacian + median kernel, and their size has been estimated using a recursive outward analysis of three circular shells, as better described in Poggianti et al. (2017b). For each star-forming knot, we then extracted the integrated spectrum, and measured both velocities (and velocity dispersions) and emission line fluxes, which have been subsequently used to characterize the ionization mechanism responsible for the Hα emission, measure the gas metallicity, and derive the ionized gas mass (as better described in Section 6). For the purpose of this paper, we used only the knots characterized by a stellar ionization mechanism (i.e. star-forming or composite regions), as characterized by MUSE emission-only line ratios (Poggianti et al. (2017b).

4 RESULTS

Figs 1–4 show for each galaxy (a) the white light image of the galaxy with an arrow pointing towards the cluster brightest cluster galaxy (BCG) (top left-hand panel), (b) the stellar kinematics (top right-hand panel), (c) the star-forming knots (lower left-hand panel) derived from the MUSE datacubes (see Section 3), and (d) the CO(2 − 1) spectra (T_{mb}^*) from the APEX data. The observed

[2]http://www.iram.fr/IRAMFR/GILDAS

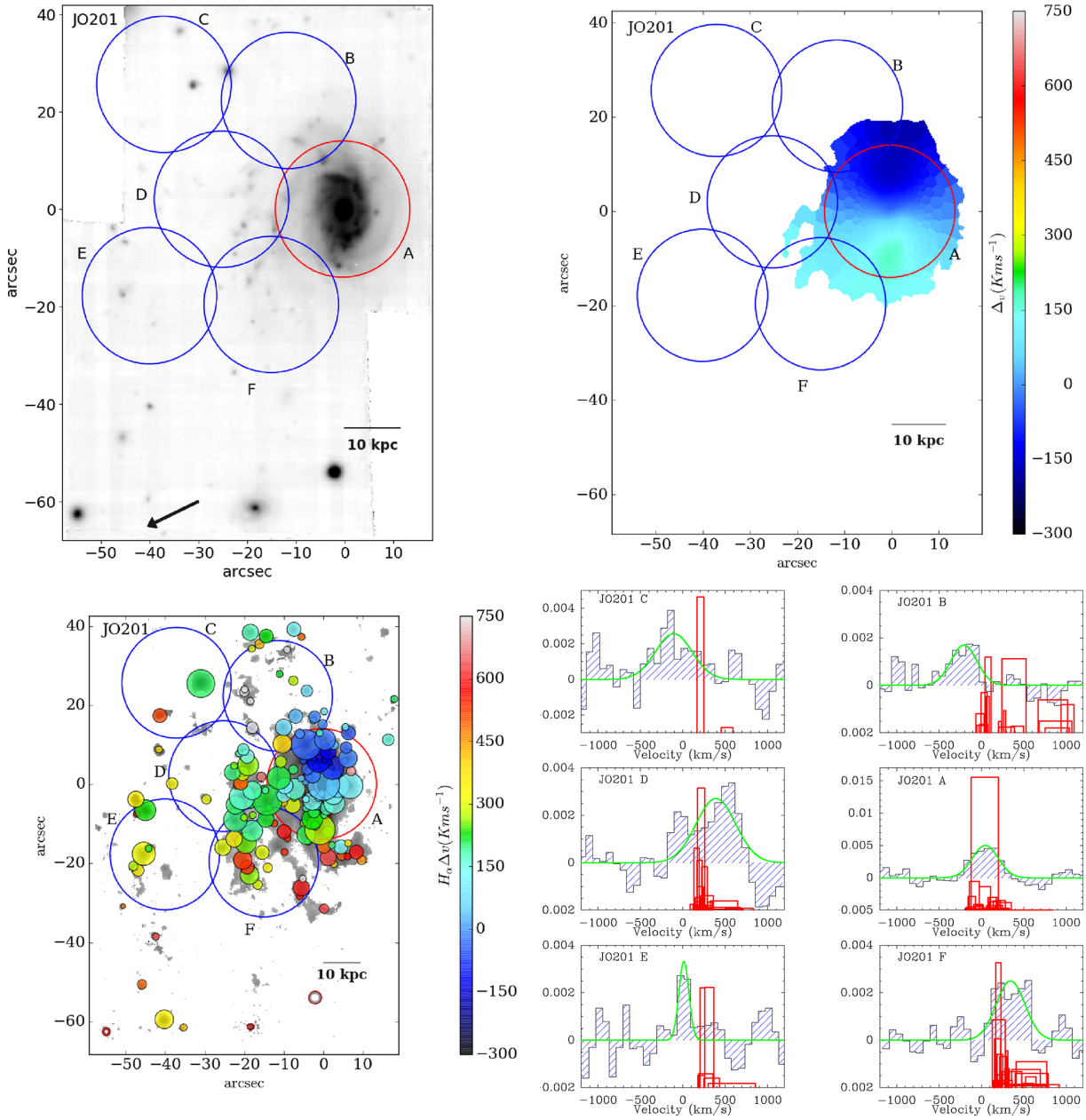

Figure 1. *JO201*: The upper left-hand panel shows the white light image of the galaxy extracted from the MUSE data cube. The upper right-hand panel shows the stellar kinematics derived from MUSE spectra in Voronoi binned regions with S/N = 10. The lower left-hand panel shows the galaxy emission determined from the continuum under the Hα emission from the MUSE data (in grey) and the star-forming knots colour coded according to their velocity with respect to the galaxy centre. Red (superimposed to the main galaxy body) and blue circles are the observed APEX pointings. The lower right-hand panels show the CO(2 − 1) spectra (T^*_{mb}) in the six positions. In each spectrum, the underlying red boxes correspond to the Hα emissions of the star-forming knots within the APEX beam (see text).

APEX pointings are overplotted on all the maps: The red circle marks the pointing superimposed to the galaxy centre, while the blue ones are positioned along the stripped tails. The grey region in the lower left-hand panels shows the galaxy emission traced by the Hα line for spaxels with an S/N > 5, while the coloured circles correspond to the star-forming knots described in Section 3. Their colour corresponds to the velocity relative to the galaxy centre (and to the zero velocity of APEX observations). The red boxes in the lower right-hand panels indicate the ionized gas velocity of the star-forming regions, with an height proportional to the Hα flux, normalized using different scales for the purpose of visualization, and a width corresponding to the Hα velocity dispersion. The APEX pointings outside of the galaxy discs extend between ∼20 and ∼67 kpc (in JO206) and are superimposed to regions where at least one Hα emitting region is present.

4.1 JO201

JO201 is one of the most spectacular jellyfish galaxies revealed by the GASP survey: It is moving at high velocity in the A85 cluster mostly along the line of sight ($\Delta v_{\rm cl} = -3363.7\,{\rm km\,s^{-1}}$, i.e. $\sim 3.4\sigma_{\rm cl}$), so that in the outskirts of the disc (starting from ∼6 kpc

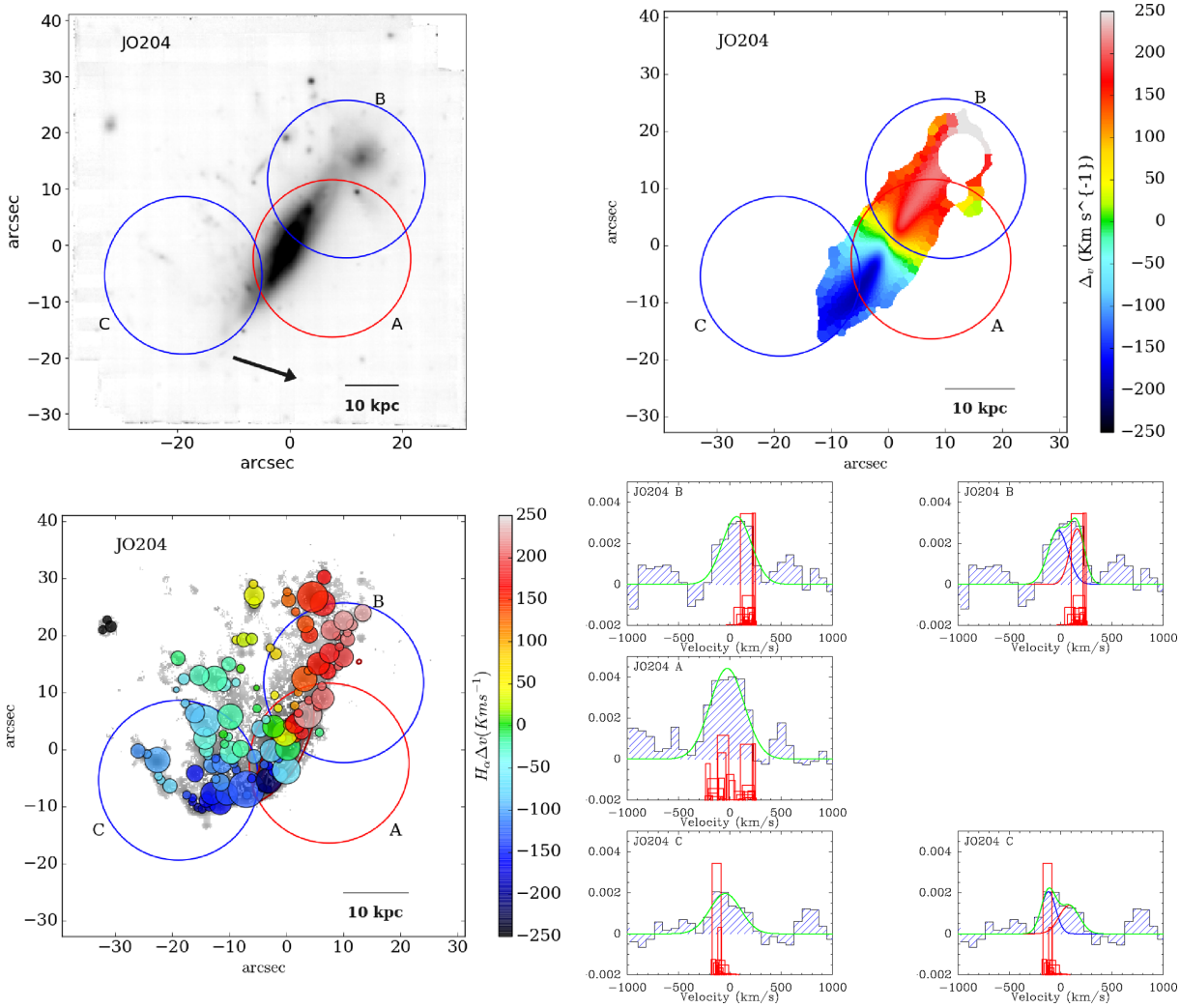

Figure 2. *JO204*: The upper left-hand panel shows the white light image of the galaxy extracted from the MUSE data cube. The upper right-hand panel shows the stellar kinematics derived from MUSE spectra in Voronoi binned regions with S/N = 10. The lower left-hand panel shows the galaxy emission determined from the continuum under the Hα emission from the MUSE data (in grey) and the star-forming knots colour coded according to their velocity with respect to the galaxy centre. Red (superimposed to the main galaxy body) and blue circles are the observed APEX pointings. The lower right-hand panels show the CO(2 − 1) spectra ($T^*_{\rm mb}$) in the three positions. The two right-hand panels show the double Gaussian fit. In each spectrum, the underlying red boxes correspond to the Hα emissions of the star-forming regions within the APEX beam (see text).

from its centre) the ionized gas is increasingly redshifted. This indicates the presence of gas trailing behind the stellar component (Bellhouse et al. 2017). This galaxy lies at a projected radial distance from the cluster BCG of 0.15 × R_{200} (i.e. at about 360 kpc). Our procedure revealed the presence of 148 Hα emitting knots, 122 of them being classified as star forming. Their median ionized gas mass is 1×10^6 M$_\odot$ and in total they account for 9.57×10^7 solar masses of ionized gas.

Fig. 1 shows the CO detections in the six pointings of JO201. The pointing A encompasses the galaxy centre, and its CO velocity distribution is coincident with the one of the Hα emission from the SF knots.

The velocities of the molecular gas and the ionized gas are instead only partially coincident in the pointings D and F, though in the D pointing the CO peak is measured with a quite low S/N (3.1, see Table 3). The other external pointings (B, C, and E) reveal the presence of molecular gas at a velocity that is different from that of the ionized gas. In particular, we were able to identify in the C and E pointings only a few H II regions/complexes, and they have a positive velocity with respect to the galaxy centre, while the peak of the CO is negative (−107 km s^{-1}, pointing C) or consistent with a zero velocity (12 km s^{-1}, pointing E). Moreover, in the C pointing, where also the ionized gas is only marginally detected, the S/N of the CO detection is low (2.2).

Given the discrete distribution of the Hα emission within the APEX beams, possibly coincident with CO concentrations, for all the pointings except the central one we also performed a double Gaussian fit, fixing the peak velocity to the value of the corresponding Hα emission when a free fit did not recover the line. The results are also given in Table 3. The asterisk marks the parameter fixed for the double fitting procedure. By imposing a double Gaussian fit, the significance of the secondary peak in the D pointing increases (S/N = 3.4), while it remains low in the C pointing.

The behaviour of cold gas in JO201 is rather complex. Pointings B and F partly cover the outer parts of the disc, and the CO emission

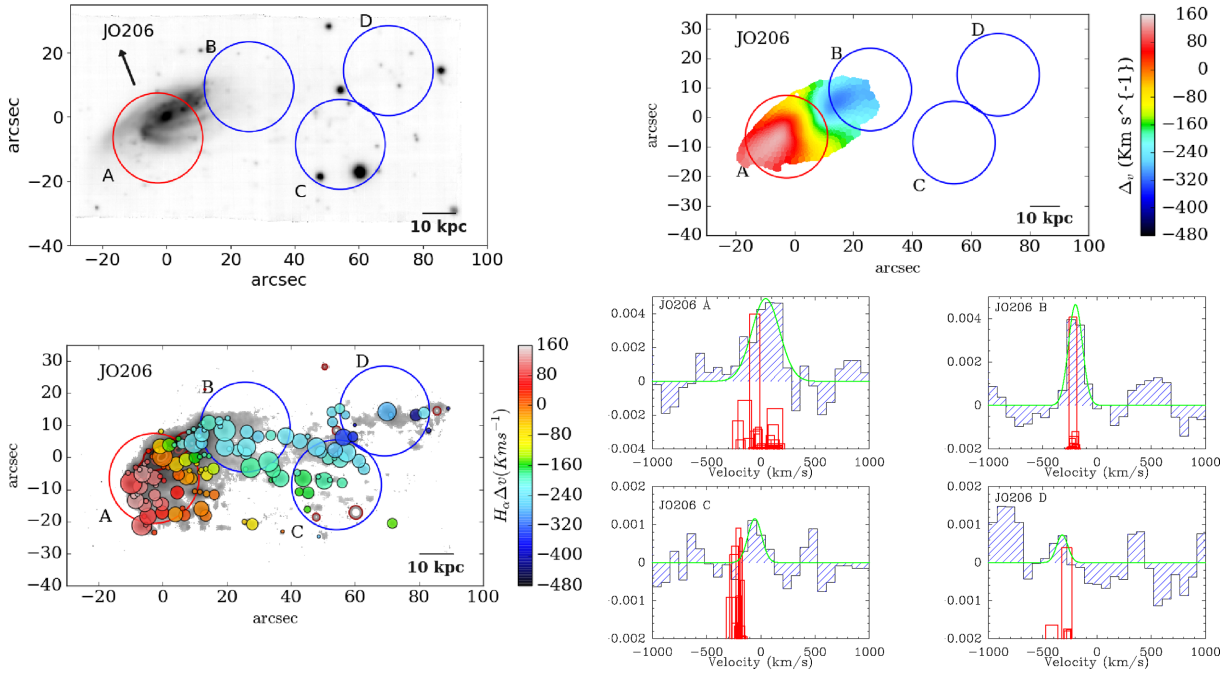

Figure 3. *JO206*: The upper left-hand panel shows the white light image of the galaxy extracted from the MUSE data cube. The upper right-hand panel shows the stellar kinematics derived from MUSE spectra in Voronoi binned regions with S/N = 10. The lower left-hand panel shows the galaxy emission determined from the continuum under the Hα emission from the MUSE data (in grey) and the star-forming knots colour coded according to their velocity with respect to the galaxy centre. Red (superimposed to the main galaxy body) and blue circles are the observed APEX pointings. The lower right-hand panels show the CO(2 − 1) spectra ($T^*_{\rm mb}$) in the four positions. In each spectrum, the underlying red boxes correspond to the Hα emissions of the star-forming regions within the APEX beam (see text).

is compatible with the disc rotation i.e. it is redshifted in F and blueshifted in B. However, the F pointing CO detection displays a double peak, which overlaps with the double-peaked Hα emission: one at a velocity similar to the stellar velocity of the closest region on the disc and a secondary one clearly trailing behind. This seems to indicate that within the pointings superimposed on the main galaxy disc part of the molecular gas is still linked to the stellar/gaseous disc rotation, while part of it follows the stripped gas where new stars are born (traced by part of the H II knots).

Some molecular gas associated with the disc rotation is found also in the pointing D, where a secondary peak likely indicates the presence of a stripped component accelerated by the ram pressure.

Coming to the more external pointings, pointing C has only a very tentative detection (S/N = 2.2, see Table 3) while the CO detection in E is more secure (S/N = 3.8). Both of these pointings show cold gas emission at a different velocity with respect to the warm gas component traced by the Hα emission. In fact, the Hα emission is redshifted with respect to the centre of the stellar disc, and is only marginally associated with CO peaks. Most of the CO has a velocity that is compatible with the stellar component at the closest position on the galaxy disc, as if it was less easily stripped along the line of sight. If this is true, then in evaluating the star formation efficiency (SFE) within the APEX beams, we would have to consider only the CO-emitting gas associated with the Hα emission (see Section 6).

4.2 JO204

JO204 belongs to the cluster A957 and is moving at $\sim -800\,{\rm km\,s^{-1}}$ with respect to the cluster (i.e. $\sim 1.25\sigma_{\rm cl}$). It is located very close to the cluster centre, at $0.08R_{200}$ ($\sim$132 kpc). JO204 is probably at its first infall in the A957 cluster (Jaffé et al. 2018) and is mostly being stripped on the plane of the sky, as demonstrated by the coherent rotation of the stripped gas with respect to the undisturbed stellar component (shown in the upper right-hand panel of Fig. 2).

It possesses 92 star-forming knots, according to the procedure described in Section 3 (see also Gullieuszik et al. 2017), but only 51 of them have S II lines measurements within the range where the Proxauf, Öttl & Kimeswenger (2014) calibration can be applied. The average ionized gas mass in these knots turns out to be $5.3 \times 10^4\,{\rm M}_\odot$, and the total ionized gas mass within these star-forming knots is $1.8 \times 10^7\,{\rm M}_\odot$ (one order of magnitude smaller than the JO206 galaxy, see Section 4.3).

As for the CO emission, shown in Fig. 2, lower right-hand panels, it is again consistent with the overall distribution of the ionized gas in the central pointing [containing an active galactic nucleus (AGN) also in this case], while in the two external slightly off-disc regions the CO line is wider than the Hα emission and a double Gaussian fit (shown in the two lower right-hand panels) reveals that the CO is again showing probably a double component: one that is coincident in velocity with the Hα emission and another one moving at a lower absolute velocity value.

In this case, the galaxy is moving in the plane of the sky, and the net effect of the gas stripping on the velocity of the molecular gas is less easily seen. What we see is, in fact, the combination of the RPS and the galaxy rotation.

4.3 JO206

JO206 belongs to the low-mass cluster IIZW108 and lies at $\sim$0.3 R_{200} from the BCG ($\sim$351 kpc). It differential velocity with respect to the cluster is $\sim 800\,{\rm km\,s^{-1}}$ (i.e. $\sim 1.5\sigma_{\rm cl}$). JO206 is the GASP galaxy showing the longest ionized gas tails (Poggianti et al. 2017b),

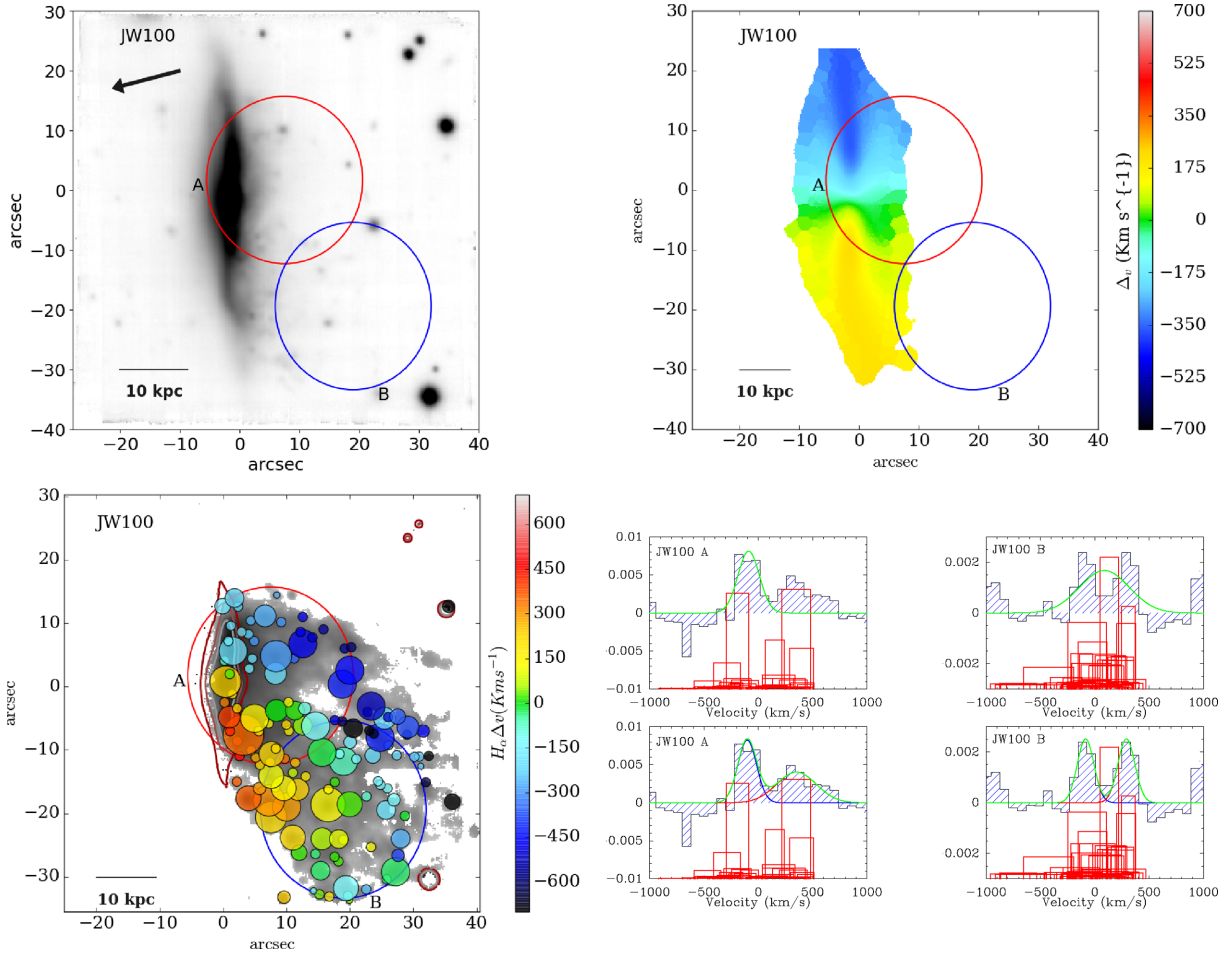

Figure 4. *JW100*: The upper left-hand panel shows the white light image of the galaxy extracted from the MUSE data cube. The upper right-hand panel shows the stellar kinematics derived from MUSE spectra in Voronoi binned regions with S/N = 10. The lower left-hand panel shows the galaxy emission determined from the continuum under the H α emission from the MUSE data (in grey) and the star-forming knots colour coded according to their velocity with respect to the galaxy centre. Red (superimposed to the main galaxy body) and blue circles are the observed APEX pointings. The lower right-hand panels show the CO(2 − 1) spectra ($T^*_{\rm mb}$) in the two positions (top row), while the bottom row shows the 2-Gaussian fit of the emission line spectra. In each spectrum, the underlying red boxes correspond to the H α emissions of the star-forming regions within the APEX beam (see text).

where 139 knots of SF has been revealed through their H α emission. With the exception of the central knot showing line ratios typical of AGN emission, almost all the other knots are consistent with being ionized by young stars formed *in situ*. Their median ionized gas mass is $\sim 1.5 \times 10^5$ M$_\odot$, and their total mass is $\sim 1.7 \times 10^8$ M$_\odot$, not including the diffuse H α emission and the regions where the gas density could not be estimated using the [S II] 6716/[S II] 6732 ratio. Our detections of the CO line, shown in Fig. 3, are significant (S/N > 3) for the central pointing and for the region located at ∼30 kpc from the centre (pointing B). A free gaussian fit in the C and D pointings was not able to recover the molecular line, and we had to impose a peak position (-55 km s^{-1} for the C pointing, -320 km s^{-1} for the D pointing) in order to get the fit. If real, in C and D again the molecular gas appears to be at a different velocity with respect to the H α emission. In any case, the C pointing is only marginally significant (S/N = 2.5, $T_{\rm ON}$ = 93 min), and the farthest D pointing (at ∼67 kpc) is consistent with a non-detection. We notice, however, that the observations of both these pointings are shorter than what we asked for and longer exposures would be needed to ascertain the amount of molecular gas beyond ∼40 kpc from the galaxy main body.

4.4 JW100

JW100 (also known as IC5337) is a galaxy located close to the centre of the cluster A2626 (at ∼0.05 R_{200}, i.e. 86 kpc), and it is moving at a velocity $v \sim 1560$ km s^{-1} with respect to the cluster velocity (i.e. $\sim 2.6\sigma_{\rm cl}$). Gitti (2013) detected it in radio continuum using the Very Large Array and suggested that it is a head–tail radio galaxy, whose radio morphology is therefore linked to the ram-pressure effects. We have selected it as a candidate jellyfish on the basis of its appearance in the *B*-band images of the WINGS survey (Fasano et al. 2006; Moretti et al. 2014; Poggianti et al. 2016). It turns out, in fact, that this galaxy is a real jellyfish galaxy (Sanchez et al., in preparation), and it also possesses an AGN at its centre (Poggianti et al. 2017a). We identified 106 star-forming knots (among the 131 total knots) with a median mass of 0.8×10^6 M$_\odot$, accounting for a total mass of ionized gas of 5.63×10^7 solar masses. We observed it with APEX using the two pointings A and B shown in the left-hand panel of Fig. 4, one (A) containing almost all the galaxy disc and the other (B) along the most prominent tail. As can be seen from Fig. 4, right-hand panels, both pointings reveal the presence of molecular gas and neither of them can be well fitted with a single Gaussian

Table 3. For each APEX pointing we give the 1 σ RMS in mK, the S/N, the peak CO velocity in km s^{-1}, the main beam temperature in mK, the FWHM in km s^{-1} and the total CO flux within the fitted line in Jy km s^{-1}. The last two columns refer to the corresponding H_2 mass calculated assuming the Milky Way CO-to-H_2 conversion factor and the metallicity dependent CO-to-H_2 conversion factor from Accurso et al. (2017).

Gx	Pointing	RMS (mK)	S/N	Rel. vel. (km s^{-1})	T_{mb} (mK)	FWHM (km s^{-1})	CO flux (Jy km s^{-1})	$M(H_2)$MW (10^9 M$_\odot$)	$M(H_2)$ (10^9 M$_\odot$)
JO201	A	0.9	5.4	46	5.0	360.7	75.15	9.60	6.59
JO201	B	0.5	3.2	−207	1.7	363.0	25.55	3.26	2.24
JO201	C	1.2	2.2	−107	2.6	510.4	54.44	6.96	5.69
	C1		2.6	−177	3.2	278.7	36.74	4.69	3.84
	C2		1.4	154	1.7	200.0*	14.48	1.85	1.51
JO201	D	0.9	3.1	390	2.7	548.7	61.74	7.89	5.41
	D1		2.3	−6	2.2	249.9	22.56	2.88	1.98
	D2		3.6	484	3.4	336.7	47.34	6.05	4.15
JO201	E	0.9	3.8	12	3.3	139.4	19.18	2.45	1.72
	E1		3.6	11	3.4	128.5	18.35	2.35	1.64
	E2		0.8	300*	0.8	221.9	7.42	0.95	0.66
JO201	F	0.6	4.3	344	2.5	400.7	41.57	5.31	3.64
	F1		4.4	298	2.4	344.6	34.66	4.43	3.04
	F2		3.8	529	2.1*	80.6	7.03	0.90	0.62
JO204	A	1.0	4.3	−26	4.4	392.8	72.11	8.29	5.69
JO204	B	1.0	3.3	67	3.3	333.9	45.79	5.26	3.61
	B1		3.2	−26	2.6	229.3	25.13	2.89	1.98
	B2		3.3	160*	2.7	171.2	19.30	2.22	1.52
JO204	C	0.6	3.4	−45	2.0	353.8	28.87	3.32	2.28
	C1		3.5	−120*	2.0	167.3	14.24	1.64	1.12
	C2		2.4	83	1.4	232.2	13.36	1.54	1.05
JO206	A	1.0	4.6	45	4.9	302.8	61.46	10.43	7.16
JO206	B	0.9	5.0	−198	4.6	151.2	29.14	4.95	3.39
JO206	C	0.5	2.5	−55*	1.2	149.7	7.19	1.22	1.13
JO206	D	0.7	1.0	−320*	0.7	123.7	3.73	0.63	0.91
JW100	A	2.4	3.3	−89	8.1	233.4	78.97	19.17	13.15
	A1		4.2	−102	8.2	204.1	69.86	16.96	11.63
	A2		2.1	350	4.0	427.2	71.71	17.41	11.94
JW100	B	0.7	2.3	89	1.7	540.4	37.60	9.13	6.26
	B1		3.9	−84	2.5	180.5	18.86	4.58	3.14
	B2		3.9	291	2.5	184.8	19.33	4.69	3.22

component. Both pointings require two gaussian profiles, almost coincident with the two peaks of Hα emission and having similar CO fluxes (lower right-hand panels in Fig. 4).

In this case, the velocities of the two components of warm ionized gas and cold CO emitting gas are well correlated.

4.5 Overall CO and Hα emission

To summarize, significant CO detections are found in the discs of all four galaxies. Other significant detections are found in the pointings neighbouring the galaxy discs (B, D, and F in JO201, B in JO206, and B and C in JO204) and well outside of the disc in pointings E of JO201 and B of JW100. Only tentative detections are found in C of JO201 and C and D of JO206.

In the tails of our jellyfish galaxies, the velocities of significant CO detections overlap (fully or in part) with the velocities of the Hα-emitting knots within that beam (JO201 D and F, JO204 B and C, JO206 B, and JW100 B), except for the galaxy in our sample with a very strong line-of-sight velocity component, JO201, whose CO detections in pointings B, C, and E have no overlap in velocity between CO and Hα.

The generally good coincidence between CO and Hα emission is consistent with the molecular gas we detect in the tails representing the gas reservoir out of which SF takes place. Additional CO velocity components in these pointings are most probably indicating a differential effect of the RPS on the cold and warm gas. Finally, the fact that the CO emission in the B, C, and E JO201 pointings retains the stellar velocity at the closest position in the disc but has no associated Hα is puzzling. It might suggest this molecular gas has formed from gas that has been more recently stripped and has either not yet formed stars or will never form stars.

It is hard to assess based only on kinematical considerations whether the molecular gas in the tails was formed *in situ* from the condensation of stripped neutral gas or if it was stripped in molecular form. Given the expected lifetimes of molecular clouds (a few Myr, Elmegreen 2000) and the large galactocentric distances

at which we observe the CO, the most plausible hypothesis is in-situ formation within the stripped tails. Moreover, the average molecular gas content in spiral galaxies is ∼10 per cent (Saintonge et al. 2011), and this is consistent with our findings in the pointings encompassing the galaxy light (see Section 5), which suggests that not a significant amount of molecular gas is missing within these regions (see also Kenney & Young 1989 for similar results in the Virgo cluster), making it very plausible that the molecular gas in the tails has been formed in-situ.

5 H_2 MASSES

We derived the H_2 masses using the formulation by Watson & Koda (2017), i.e.

$$\left(\frac{M_{H_2}}{M_\odot}\right) = 3.8 \times 10^3 \left(\frac{\alpha_{10}}{4.3}\right) \left(\frac{r_{21}}{0.7}\right)^{-1} \left(\int S_{21} dv\right) (D)^2 , \quad (1)$$

where α_{10} is the CO-to-H_2 conversion factor expressed in $M_\odot\,pc^{-2}$ (Bolatto, Wolfire & Leroy 2013), r_{21} is the CO $J = 2 - 1/1 - 0$ line ratio, S_{21} is the CO integrated line flux in Jy, and D is the distance in Mpc.

In calculating molecular gas masses, we used $r_{21} = 0.79$, as derived from the xCOLD GASS survey (Saintonge et al. 2017) that studies a sample of 532 galaxies in the low-z Universe with masses larger than $10^9\,M_\odot$. The value adopted is slightly larger than the usual value of 0.7 derived from resolved observations of nearby star-forming discs (Leroy et al. 2013), but lower than the value found in galaxies nuclei ($r_{21} \sim 1$, Leroy et al. 2009). As for the CO-to-H_2 conversion factor, we used both the standard Milky Way value of 4.3 (already including the helium content, Leroy et al. 2011) (9th column of Table 3) and the one derived assuming the analytical dependence on the metallicity found in Accurso et al. (2017), neglecting the small dependence on the distance from the main sequence of SF (i. e. the locus of the star-forming galaxies in the SFR versus $M_\star$ plane), since our values do not refer to the whole galaxy (10th column of Table 3). This relation is valid in the range $7.9 < (12 + \log(O/H)) < 8.8$, while most of the gas in our APEX pointings turned out to possess a metallicity larger than 8.8. When the metallicity within the APEX pointing was larger than 8.8, we, therefore, used the value derived assuming 12+log(O/H) = 8.8 (where $\alpha_{CO} = 2.95$), as suggested by Accurso et al. (2017). In fact, our galaxies have all large metallicities/masses, and we expect them not to suffer from the usual problems related to the conversion factor in low metallicities galaxies.

In all galaxies, we were able to measure large amounts of cold gas both in the galaxy main body and along the tails, even if with different degrees of significance: The central pointings reveal an H_2 mass that goes from $8.29 \times 10^9\,M_\odot$ in JO204 to $19.17 \times 10^9\,M_\odot$ in JW100. We find typically a few $10^9\,M_\odot$ of molecular gas in each of the APEX beams, covering the off-disc regions, although with values of $S/N < 3$ in some cases. In the most distant position in the tail of JO206, we only obtained an upper limit corresponding to $0.63 \times 10^9\,M_\odot$ of H_2.

The total amount of molecular gas detected in JO201 is high and similar to the stellar mass of the galaxy. However, as described in Section 4, a significant fraction of this molecular gas could not be associated with the stripped tails, meaning that a not negligible fraction of it is still linked to the galaxy discs. In the other three galaxies, the molecular gas mass fraction is lower (0.42, 0.20, and 0.14 in JO204, JO206, and JW100, respectively, assuming the Galactic value of the CO-to-H2 conversion factor).

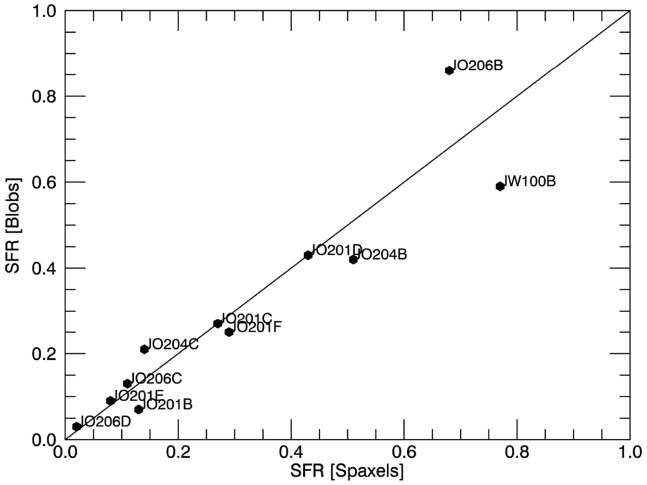

Figure 5. Comparison between the SFR measured from the star-forming regions and from the single star-forming spaxels within each APEX pointing.

6 STAR FORMATION EFFICIENCY

The most widely used way to identify the conditions at which gas is able to form stars is to evaluate the so called SFE, which is the ratio between the SFR surface density and the H_2 surface density. This SFE is the inverse of the H_2 gas depletion time, i.e. the time needed to consume the available H_2 at the current SFR. This means, for example, that if 1per cent of the H_2 is converted into stars every 10^8 years, then the SFE is $10^{-10}\,yr^{-1}$.

In order to estimate the SFE in the different APEX pointings, we used the molecular gas masses derived in Section 5 normalized to the APEX beam area (HPBW), and the resolved SFR inferred from the MUSE data cubes as follows. We first corrected the MUSE data cubes for the stellar absorption modelled using the SINOPSIS code (Fritz et al. 2017), and then run the KUBEVIZ code (Fossati et al. 2016) on the emission-only MUSE data cube to measure all the relevant emission lines that have been used to estimate the Balmer decrement to correct for the dust extinction and classify each spaxel on the basis of the ionization mechanism using the BPT diagram (Baldwin, Phillips & Terlevich 1981), following the procedure described in Poggianti et al. (2017b).

The SFR within each APEX pointing has been computed from the Hα luminosity (corrected for dust and stellar contribution) using the Kennicutt (1998)'s relation

$$SFR = 4.6 \times 10^{-42} L_{H\alpha}, \quad (2)$$

where the SFR (for a Chabrier 2003 IMF) is given in solar masses per year and the Hα luminosity is in erg per second. In these calculations, we only used spaxels classified as either pure star forming or located in the so called Composite region in the O[III]/Hβ versus N[II]/Hα BPT diagram, using the demarcation lines by Kewley et al. (2001) and Kauffmann et al. (2003). We also estimated the total SFR within each APEX beam by summing the contribution of each star-forming knot found using the procedure described in Poggianti et al. (2017b), finding very similar values (see Fig. 5). This means that most of the SF in the galaxy tails takes place within the knots.

Before evaluating the SFE, which depends on the assumptions on the α_{CO} and the r_{21}/r_{10} factors, we compared the Hα fluxes measured from the MUSE data within the beam with the total CO flux that we measured. This is shown in Fig. 6, where black dots refer to our data, while red dots are values taken from Jachym

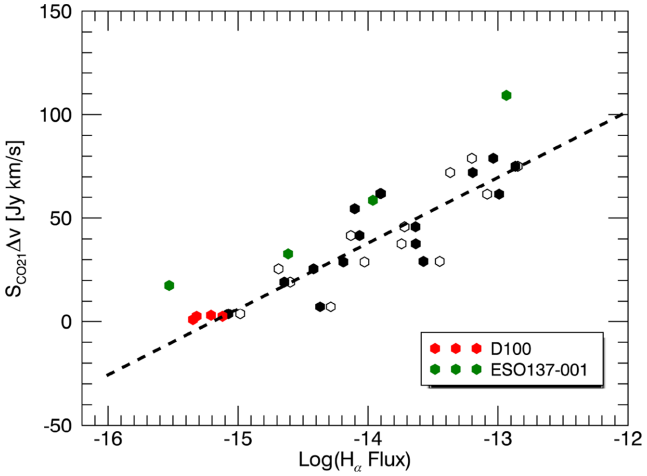

Figure 6. CO fluxes from APEX data against H α fluxes (in erg s^{-1}) derived from GASP/MUSE observations: black filled symbols refer to H α fluxes measured from individual spaxels, empty symbols refer to H α fluxes measured from the sum of individual star-forming knots, in both cases classified as star-forming or composite. Red and green symbols are literature values for other two nearby jellyfish galaxies, D100 and ESO137 − 001, respectively, from Jachym et al. (2017) and Jáchym et al. (2014).

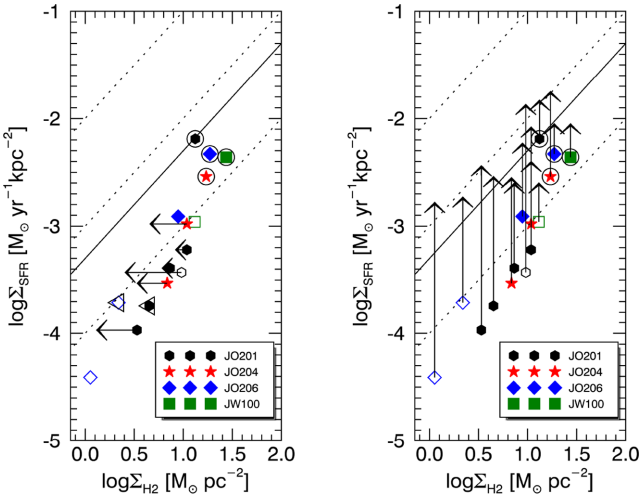

Figure 7. SFR surface density, Σ_{SFR}, derived following equation (2) as a function of molecular gas surface density, Σ_{H_2}, estimated from CO(2 − 1) emission from APEX for the different pointings along the tails and in the main body of the jellyfish galaxies: Black dots refer to JO201, red stars refer to JO204, blue diamonds refer to JO206, and green squares refer to JW100. Empty symbols indicate CO detections with S/N < 3. The four symbols showing the highest SFRs indicate the measurements in the main body of our galaxies (also enclosed within a circle). Dotted lines represent fixed H_2 depletion times in years (10^8, 10^9, and 10^{10} from the top to bottom), while the continuous line shows the average depletion time found for a sample of 30 nearby disc galaxies with a resolution of 1 kpc (Bigiel et al. 2011). Arrows in the left-hand panel show molecular gas surface densities considering only the molecular gas coincident with the H α emission. The two triangles indicate pointings whose the molecular gas surface density associated with the H α emission extend beyond the plot limits. Arrows in the right-hand panel show SFRs densities calculated using the effective area covered by the H α emission.

et al. (2017) for different pointings in the D100 galaxy in the Coma cluster and green dots are relative to the ESO137 − 001 galaxy from Jáchym et al. (2014). The empty symbols indicate the H α flux that we measure from the H II regions identified with the MUSE data. We find that a linear relation links the CO fluxes (in Jy km s^{-1}) in our stripped tails and the H α luminosities (in erg s^{-1}), i.e.

$$S_{\rm CO21}\,\Delta v = 483.3 + 31.8 \times \log({\rm H}\,\alpha). \quad (3)$$

This is true both when we consider the integrated H α luminosity of each spaxel classified as H II region or composite, and if we consider the contribution of each individual H II region within the APEX beam. This relation holds independently of the galaxy masses, given the large range of galaxy masses involved in the plot (from the 2×10^9 of D100 to 3×10^{11} in JW100). This means that the mechanism producing the ionizing flux (probably SF) is strictly linked to the molecular gas available.

All the galaxies presented here are high-mass ($\geq 4 \times 10^{10}\,M_\odot$) galaxies and are among those experiencing the most intense stripping in GASP, due to their low distance and high velocity with respect to the cluster centre (Jaffé et al. 2018). In Bellhouse et al. (2017), Gullieuszik et al. (2017), and Poggianti et al. (2017b), we have estimated the ram pressure experienced by three of our galaxies (JO201, JO204, and JO206, respectively), finding the highest value for JO201, which is a galaxy crossing the dense core of a massive cluster, and increasingly lower values for JO204 and JO206, which reside in lower mass clusters (as does JW100). In this context, it is of interest to compare the molecular gas content with respect to the stellar mass for these galaxies. Interestingly, the total mass of molecular hydrogen measured with APEX for JO201 is comparable to the total stellar mass of the galaxy (i.e. a fraction of 100 per cent). For the other galaxies, the H_2 mass fraction derived assuming the Galactic CO-to-H2 conversion factor is lower: 42 per cent, 20 per cent, and 14 per cent for JO204, JO206, and JW100, respectively. At the stellar masses of the galaxies studied, all of these fractions are above the expected gas fractions from observations (Saintonge et al. 2011) and simulations (Popping, Somerville & Trager 2014) of $z = 0$ galaxies by a factor of ∼5–15 (where the lower values are found for JO206, JO204, and JW100, while the highest value is for JO201), suggesting that RPS could be changing the phase of the gas, generating more molecular hydrogen, which, in turn, aids the formation of new stars.

Having converted the CO fluxes into molecular gas masses, we calculated the surface densities of H_2 within each APEX beam and compare them with the SFR surface density, that is shown in both panels of Fig. 7, illustrating the Kennicutt–Schmidt relation (Schmidt 1959; Kennicutt 1998). Different symbols and colours have been used for different galaxies: Black dots are for JO201, red stars are for JO204, blue diamonds are for JO206, and green squares are for JW100. The symbols enclosed within circles indicate the central pointings of each galaxy. The dotted lines in Fig. 7 represent constant depletion times of 10^8, 10^9, and 10^{10} yr from the top to bottom, while the continuous line shows the average depletion time (∼2.3 Gyr) found by Bigiel et al. (2011) for a sample of 30 nearby disc galaxies (IRAM HERACLES CO survey). The SFR densities that we measure in the stripped tails are very low, or equivalently the gas depletion times are very long, meaning that it will take longer than the Hubble time to consume the molecular gas in the tails with the current SFR. Our results are in agreement with what has been found in other ram-pressure stripped galaxies (Jáchym et al. 2014; Verdugo et al. 2015; Jachym et al. 2017), and imply that most of the molecular gas in the tails will not be used to fuel the SF, but will ultimately get dispersed into the ICM.

However, while the APEX beam size does not allow to resolve the location of the CO emitting region, we do have from MUSE

data the ability to distinguish the Hα location, with a resolution of ∼1 kpc (Poggianti et al. 2017b). Therefore, we can make two working hypothesis: Either (a) the Hα and CO emission come from co-spatial gas phases, and in this case we should calculate a partially resolved CO emission using only the CO component that is coincident in velocity with the Hα peaks, or (b) the two phases might not be strictly linked (due to a more diffuse CO or Hα emission), and in this case we can evaluate each indicator with respect to the covered area that we can estimate with our data. This means assuming a diffuse CO emission over the whole APEX beam, and a clumpy Hα emission traced by the star-forming knots. The arrows in the left-hand panel of Fig. 7 illustrate case (a), and indicate the H_2 surface densities obtained using the masses corresponding to the gaussian fit of the CO line coincident in velocity with the Hα knots. The two triangles indicate pointings where the H_2 surface density calculated in this way extends beyond the plot limits. The arrows in the right-hand panel of Fig. 7 refer, instead, to the case (b) i.e. using the effective area covered by the Hα emission in evaluating the SFR surface density (while the H_2 surface density does not change). In both cases, the extremely low SFE characterizing the stripped tails are brought back to the depletion times expected for normal star-forming galaxies. In other words, our results seem to indicate that the SF can proceed normally within the stripped tails, but only a resolved study on the CO emission will definitively answer this question. If, instead, the whole amount of molecular gas is clumpy as the Hα, the points will fall back to low SFE. Moreover, if this molecular gas is formed *in situ*, it could be not associated with H II regions, as it is the case for D100 (Jachym et al. 2017) and ESO137-001 (Jáchym et al. 2014), and this would again points towards a low SFE. We will discuss this possibility in a forthcoming paper studying the same sample of jellyfish galaxies with ALMA observations.

Finally, we can calculate the total amount of ionized gas using the Hα fluxes measured with MUSE. In order to get the total mass of ionized gas within the APEX beam, we used equation (3) from Poggianti et al. (2017b), which requires an estimate of the electron density n. To derive it, we used the ratio between the red S II lines at 6716 and 6732 Å (excluding spaxels with a S/N below 3 in both lines) and the calibration by Proxauf et al. (2014) (valid in the range $0.4 < [\mathrm{S\,II}]6716/[\mathrm{S\,II}]6732 < 1.435$). Moreover, since SF is known to take place within H II regions, we did not derive the electron density for each spaxel, but for each H II region/complex identified within the APEX beam. We then sum up all the evaluable masses in each beam to obtain the total mass of ionized gas to be compared with the H_2 mass. Fig. 8 shows that the ratio between the mass already ionized by SF and the available molecular gas mass within each APEX beam is $\sim 0.1\text{–}0.2 \times 10^{-2}$, which is one order of magnitude smaller than the one found by Jachym et al. (2017) along the tail of a smaller jellyfish galaxy (even though the central regions of JO201 and JO206 show more compatible results). Our determinations, however, are based only on star-forming regions where the S II doublet was measurable and within the range of the adopted calibration; therefore, our values have to be taken as lower limits. Moreover, if we consider only the H_2 mass associated with the Hα emission, the results are shifted towards higher values, as indicated by the arrows.

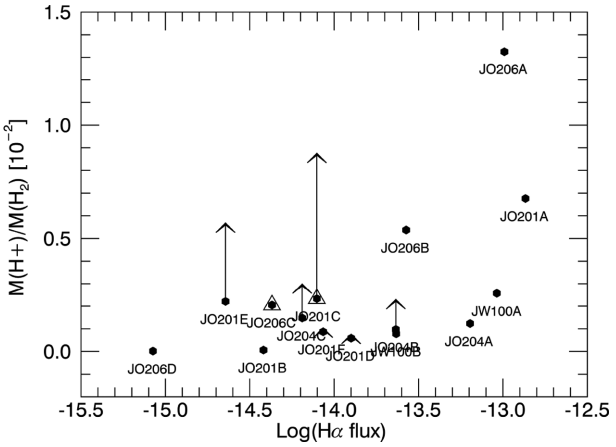

Figure 8. Ratio between the mass of ionized and molecular hydrogen within each APEX beam versus the total Hα flux within the beam. The arrows indicate the ratios obtained by using only the H_2 masses associated with the Hα emission. Symbols within the triangles indicate pointings whose ratio between the two gas masses extends beyond the plot limits.

7 SUMMARY AND CONCLUSIONS

We have studied a sample of four jellyfish galaxies from the GASP sample (Poggianti et al. 2017b) with the APEX telescope to derive the molecular gas content both in the galaxy main bodies and along the stripped tails through the CO(2 − 1) emission. Similar studies have been performed so far only in three nearby jellyfish galaxies (Jáchym et al. 2014; Verdugo et al. 2015; Jachym et al. 2017) in Norma, Virgo, and Coma clusters, respectively. Our galaxies lie at higher redshifts (∼0.05), and are characterized by larger stellar masses. All of them are galaxies subject to peak stripping (Jaffé et al. 2018), even though with a different stripping efficiency. Our APEX CO observations demonstrate the following:

(i) Large amounts of molecular gas are present in the disc of our jellyfish galaxies ($8\text{–}20 \times 10^9\ M_\odot$), compatible with the values expected in normal star-forming galaxies (Saintonge et al. 2011).

(ii) Also, some of the pointings located along the stripped tails show a significant amount of molecular gas up to large distances (up to 40 kpc from the disc), while some of the tail detections are only tentative.

(iii) The total mass of molecular gas that we measure for each galaxy by summing all the pointings goes from 15 per cent to 100 per cent of the galaxy stellar mass measured from the integrated spectrum within the stellar isophote encircling the galaxy main body as traced by the continuum under the Hα emission down to 1σ above the background of our MUSE data cubes. Interestingly, the galaxy where the stripping is stronger and/or advanced (JO201) also possesses the largest fraction of molecular gas.

(iv) There is a clear correlation between the CO(2 − 1) fluxes and the Hα fluxes measured within each beam, indicating that the ionized emission and the amount of molecular gas are well linked.

(v) There is a shift between the Hα and the CO velocities in the tails, probably due to the differential effect of the ram pressure on cold and warm gas. This conclusion is, however, only preliminary, since the APEX beam contains many Hα knots, each one with its own velocity, therefore hampering a clear correspondence between the two gas phases.

(vi) The central regions of each galaxy (encircled points in Fig. 7) show average SFEs, corresponding to the typical depletion times found for nearby discs (Leroy et al. 2011), while along the stripped tails the situation dramatically changes: The SFE is very low and the depletion times imply that most of the molecular gas will not be converted into stars before joining the ICM, confirming the results already found in other nearby jellyfish galaxies (Jáchym et al.

2014; Verdugo et al. 2015; Jachym et al. 2017). However, our SFR derivation is based on the resolved Hα emission (on a kpc scale) from the MUSE data, and it is, therefore, possible to normalize the SFR to the effective area covered by this emission. This would then represent the limit case in which the CO emission is diffuse within the entire APEX beam, while only part of it is contributing to the SF that is concentrated in the smaller H II regions/complexes traced by Hα emission (Shetty, Clark & Klessen 2014; Mogotsi et al. 2016). Moreover, the joint kinematic analysis of the CO, and the resolved Hα emission suggests that our values of SFE are consistent with the ones shown by normal disc galaxies, if we consider only the molecular gas associated with the warm phase. However, since the distribution of the CO emission within the APEX beams is not known, this will be probed directly using our ongoing resolved ALMA observations of the CO emission.

This work demonstrates that galaxies subject to the RPS effect in nearby clusters of galaxies (at redshift $\sim$0.05) show tails of multicomponent gas, where the molecular gas is not negligible and act as the needed reservoir to form a new generation of stars that is linked to the ionized gas emission. Given that the central pointings reveal the presence of molecular gas masses compatible with the one of normal disc galaxies, we suggest that the molecular gas in the tails should have been formed *in situ* from the stripped neutral gas. ALMA observations of these galaxies (undergoing) will help clarifying whether this scenario is confirmed.

ACKNOWLEDGEMENTS

We thank the anonymous referee for a careful reading of this paper. We thank Carlos De Breuck, Palle Møller, and the APEX team for their support. Based on observations collected by the European Organisation for Astronomical Research in the Southern Hemisphere under ESO program 098.B-0657 and 099.B-0063 (APEX) and 196.B-0578 (VLT/MUSE). We acknowledge funding from the INAF PRIN-SKA 2017 program 1.05.01.88.04. YLJ acknowledges support from CONICYT PAI (Concurso Nacional de Inserción en la Academia 2017) No. 79170132. BV acknowledges the support from an Australian Research Council Discovery Early Career Researcher Award (PD0028506). This work made use of the KUBEVIZ software, which is publicly available at http://www.mpe.mpg.de/dwilman/kubeviz/.

REFERENCES

Accurso G. et al., 2017, MNRAS, 470, 4750
Baldwin J. A., Phillips M. M., Terlevich R., 1981, PASP, 93, 5
Balogh M. L., Navarro J. F., Morris S. L., 2000, ApJ, 540, 113
Bellhouse C. et al., 2017, ApJ, 844, 49
Bigiel F., Leroy A., Walter F., Brinks E., de Blok W. J. G., Madore B., Thornley M. D., 2008, AJ, 136, 2846
Bigiel F., Walter F., Blitz L., Brinks E., de Blok W. J. G., Madore B., Madore B., 2010, AJ, 140, 1194
Bigiel F. et al., 2011, ApJ, 730, L13
Boissier S. et al., 2008, ApJ, 681, 244
Bolatto A. D., Wolfire M., Leroy A. K., 2013, ARA&A, 51, 207
Boselli A., Gavazzi G., 2006, PASP, 118, 517
Boselli A., Gavazzi G., Lequeux J., Buat V., Casoli F., Dickey J., Donas J., 1997, A&A, 327, 522
Bosma A., 1981, AJ, 86, 1825
Byrd G., Valtonen M., 1990, ApJ, 350, 89
Cappellari M., Copin Y., 2003, MNRAS, 342, 345
Cappellari M., Emsellem E., 2003, PASP, 116, 138
Casasola V., Hunt L., Combes F., García-Burillo S., 2015, A&A, 577, A135
Chabrier G., 2003, PASP, 115, 763
Chung A., van Gorkom J. H., Kenney J. D. P., Crowl H., Vollmer B., 2009, AJ, 138, 1741
Consolandi G., Gavazzi G., Fossati M., Fumagalli M., Boselli A., Yagi M., Yoshida M., 2017, A&A, 606, A83
Cortese L., Gavazzi G., Boselli A., Iglesias-Paramo J., 2004, A&A, 416, 119
Cowie L. L., Songaila A., Hu E. M., Cohen J. G., 1996, AJ, 112, 839
Cucciati O. et al., 2006, A&A, 458, 39
Dasyra K. M., Combes F., Salomé P., Braine J., 2012, A&A, 540, A112
Dessauges-Zavadsky M., Verdugo C., Combes F., Pfenniger D., 2014, A&A, 566, A147
Dressler A., 1980, ApJ, 236, 351
Elmegreen B. G., 2000, ApJ, 530, 277
Fasano G. et al., 2006, A&A, 445, 805
Fossati M., Gavazzi G., Boselli A., Fumagalli M., 2012, A&A, 544, A128
Fossati M., Fumagalli M., Boselli A., Gavazzi G., Sun M., Wilman D. J., 2016, MNRAS, 455, 2028
Fritz J. et al., 2017, ApJ, 848, 132
Fumagalli M., Fossati M., Hau G. K. T., Gavazzi G., Bower R., Sun M., Boselli A., 2014, MNRAS, 445, 4335
Gavazzi G., Boselli A., Mayer L., Iglesias-Paramo J., Vílchez J. M., Carrasco L., 2001, ApJ, 563, L23
Gavazzi G. et al., 2013, A&A, 553, A90
Gerhard O., Arnaboldi M., Freeman K. C., Okamura S., 2002, ApJ, 580, L121
Gitti M., 2013, MNRAS, 436, L84
Guglielmo V., Poggianti B., Moretti A., Fritz J., Calvi R., Vulcani B., Fasano G., Paccagnella A., 2015, MNRAS, 450, 2749
Gullieuszik M. et al., 2017, ApJ, 846, 27
Gunn J. E., Gott J. Richard I., 1972, ApJ, 176, 1
Jáchym P., Kenney J. D. P., Ržuička A., Sun M., Combes F., Palouš J., 2013, A&A, 556, A99
Jáchym P., Combes F., Cortese L., Sun M., Kenney J. D. P., 2014, ApJ, 792, 11
Jachym P. et al., 2017, ApJ, 839, 15
Jaffe Y. L., Smith R., Candlish G. N., Poggianti B. M., Sheen Y.-K., Verheijen M. A. W., 2015, MNRAS, 448, 1715
Jaffé Y. L. et al., 2018, MNRAS, 476, 4753
Kauffmann G. et al., 2003, MNRAS, 346, 1055
Kenney J. D. P., Young J. S., 1989, ApJ, 344, 171
Kenney J. D. P., van Gorkom J. H., Vollmer B., 2004, AJ, 127, 3361
Kenney J. D. P., Geha M., Jáchym P., Crowl H. H., Dague W., Chung A., van Gorkom J., Vollmer B., 2013, ApJ, 780, 119
Kennicutt R. C., 1998, ARA&A, 36, 189
Kewley L. J., Dopita M. A., Sutherland R. S., Heisler C. A., Trevena J., 2001, ApJ, 556, 121
Larson R. B., Tinsley B. M., Caldwell C. N., 1980, ApJ, 237, 692
Lee B. et al., 2017, MNRAS, 466, 1382
Leroy A. K. et al., 2009, AJ, 137, 4670
Leroy A. K. et al., 2011, ApJ, 737, 12
Leroy A. K. et al., 2013, AJ, 146, 19
Merritt D., 1983, ApJ, 264, 24
Mogotsi K. M., Blok W. J. G. d., Caldú-Primo A., Walter F., Ianjamasimanana R., Leroy A. K., 2016, AJ, 151, 15
Moore B., Ghigna S., Governato F., Lake G., Quinn T., Stadel J., Tozzi P., 1999, ApJ, 524, L19
Moretti A. et al., 2014, A&A, 564, A138
Moretti A. et al., 2017, A&A, 599, 11
Moretti A. et al., 2018, MNRAS, 475, 4055
Peng C. Y., Ho L. C., Impey C. D., Rix H.-W., 2010, AJ, 139, 2097
Poggianti B. M. et al., 2006, ApJ, 642, 188
Poggianti B. M. et al., 2016, AJ, 151
Poggianti B. M. et al., 2017a, Nature, 548, 304
Poggianti B. M. et al., 2017b, ApJ, 844, 48
Popping G., Somerville R. S., Trager S. C., 2014, MNRAS, 442, 2398
Proxauf B., Öttl S., Kimeswenger S., 2014, A&A, 561, A10
Saintonge A. et al., 2011, MNRAS, 415, 32

Saintonge A. et al., 2017, ApJS, 233, 22
Schmidt M., 1959, ApJ, 129, 243
Serra P. et al., 2013, MNRAS, 428, 370
Shetty R., Clark P. C., Klessen R. S., 2014, MNRAS, 442, 2208
Spitzer Lyman J., Baade W., 1951, ApJ, 113, 413
Sun M., Donahue M., Voit G. M., 2007, ApJ, 671, 190
Sun M., Donahue M., Roediger E., Nulsen P. E. J., Voit G. M., Sarazin C., Forman W., Jones C., 2010, ApJ, 708, 946
Tanaka M., Goto T., Okamura S., Shimasaku K., Brinkman J., 2004, AJ, 128, 2677
Tonnesen S., Bryan G. L., 2009, ApJ, 694, 789
Tonnesen S., Bryan G. L., 2012, MNRAS, 422, 1609
Toomre A., Toomre J., 1972, ApJ, 178, 623
Vassilev V. et al., 2008, A&A, 490, 1157
Verdugo C., Combes F., Dasyra K., Salomé P., Braine J., 2015, A&A, 582, A6
Vollmer B., Braine J., Pappalardo C., Hily-Blant P., 2008, A&A, 491, 455
Watson L. C., Koda J., 2017, in Knapen J. H. L. J. C., de Paz A. G., eds, Outskirts of Galaxies. Springer, Cham, p. 175
Wong T., Blitz L., 2002, ApJ, 569, 157
Yagi M., Komiyama Y., Yoshida M., Furusawa H., Kashikawa N., Koyama Y., Okamura S., 2007, ApJ, 660, 1209
Yagi M. et al., 2010, AJ, 140, 1814
Yagi M., Gu L., Fujita Y., Nakazawa K., Akahori T., Hattori T., Yoshida M., Makishima K., 2013, ApJ, 778, 91
Yagi M., Yoshida M., Gavazzi G., Komiyama Y., Kashikawa N., Okamura S., 2017, ApJ, 839, 65
Yoon H., Chung A., Smith R., Jaffé Y. L., 2017, ApJ, 838, 81
Young J. S., Scoville N. Z., 1991, ARA&A, 29, 581

This paper has been typeset from a TEX/LATEX file prepared by the author.